New Journal of Physics
The open access journal at the forefront of physics

Deutsche Physikalische Gesellschaft DPG IOP Institute of Physics

PAPER • OPEN ACCESS

Gratings with longitudinal variations in coupling coefficients: super-efficiency and unidirectionality in distributed feedback Raman fiber lasers

To cite this article: Amirhossein Tehranchi and Raman Kashyap 2020 *New J. Phys.* **22** 103022

View the article online for updates and enhancements.

You may also like

- Estimation Genetic Stability of Faba bean (*Vicia faba* L.) Genotypes in Sallahaddin Governorate
Dawood S. Madab, Majid Sh. Hamdallah and Yasieen. N. Jabor

- *(Invited)* Advanced Materials Opportunities for High Performance Redox-Flow Batteries
Mike L. Perry

- Directly diode and bi-directional pumping 6 kW continuous-wave all-fibre laser
Qirong Xiao, Dan Li, Yusheng Huang et al.

This content was downloaded from IP address 132.207.4.76 on 22/10/2021 at 20:11

New Journal of Physics
The open access journal at the forefront of physics

Deutsche Physikalische Gesellschaft DPG
IOP Institute of Physics

Published in partnership with: Deutsche Physikalische Gesellschaft and the Institute of Physics

CrossMark

OPEN ACCESS

RECEIVED
5 June 2020

REVISED
18 September 2020

ACCEPTED FOR PUBLICATION
28 September 2020

PUBLISHED
12 October 2020

Original content from this work may be used under the terms of the Creative Commons Attribution 4.0 licence.

Any further distribution of this work must maintain attribution to the author(s) and the title of the work, journal citation and DOI.

PAPER

Gratings with longitudinal variations in coupling coefficients: super-efficiency and unidirectionality in distributed feedback Raman fiber lasers

Amirhossein Tehranchi[1,*] **and Raman Kashyap**[1,2]

[1] Advanced Photonics Concepts Laboratory, Department of Electrical Engineering, Polytechnique Montreal, University of Montreal, Montreal QC, H3C 3A7, Canada
[2] Department of Engineering Physics, Polytechnique Montreal, University of Montreal, Montreal QC, H3C 3A7, Canada
[*] Author to whom any correspondence should be addressed.

E-mail: amirhossein.tehranchi@polymtl.ca

Keywords: Bragg gratings, Raman lasers, fiber optic

Abstract

We propose a technique to design highly-efficient and -unidirectional DFB Raman fiber lasers based on the engineering of the grating's coupling coefficient including a π-phase shift position in the fiber. For this purpose, first the ideal intra-cavity signal powers for different pump power levels are determined for given fiber lengths. Then, the sum and difference between the counter-propagating wave intensities at each small segment within fiber lengths are calculated resulting in determining the ideal grating's coupling functions for co- and contra-directional-pumping. The steady-state behavior of the laser using realistic parameters is finally simulated for modified coupling functions considering the Kerr nonlinearity. For a 10 W co-directional-pumped, $\sim$1 m long single-mode super-efficient DFB, a $\sim$50% increase in the laser efficiency, more than 44 dB reduction in contra-directional lasing power, $\sim$15 times drop in the peak power of intra-cavity signal and $\sim$38% decrease in the unused-pump power are found, compared to those in a standard DFB with the same coupling-length product. Although an enhanced nonlinear refractive index due to thermal gradient reduces the output power of such lasers, it is shown that the super-efficient laser presents a better performance than the standard one, under such conditions.

1. Introduction

Distributed feedback (DFB) lasers have been extensively studied and developed during the past years for their unique characteristics including narrow spectral linewidth [1–32]. DFB Raman fiber lasers are pumped by another laser to produce the required gain at the Bragg grating wavelength inscribed in the core of a fiber [1], matching the Raman Stokes shift [2]. A π-phase-shifted distributed feedback (PPS-DFB) laser, in which an optical phase of $\pi/2$ is introduced into the grating, has been widely exploited to obtain single frequency (mode) operation [1, 3]. Such π-phase-shifted gratings, already used for DFB in semiconductors [4–8] as well as rare-earth-doped-fiber lasers [9–20], have also been utilized for Brillouin [21, 22] and Raman [23–32] fiber lasers with a length of a few tens of centimeters. They have been considerably researched as promising sources in sensing as well as various applications such as wavelength conversion [32] and pump lasers for distributed gain in telecom systems [33].

During the past years, standard PPS-DFB Raman fiber lasers have been mostly demonstrated for constant-coupling uniform fiber Bragg grating (FBG) with a limited efficiency (power ratio of the output Raman signal to input pump) in which a major part of the pump power remains unused [24, 25]. Also, it has already been shown that by pumping an FBG e.g., on the left-hand side, the displacement of the π-phase-shift to the right and left of the center of the grating, results in co- and contra-pumping schemes, as major part of the generated laser power exits from the right-hand side (rhs) and left-hand side (lhs),

© 2020 The Author(s). Published by IOP Publishing Ltd on behalf of the Institute of Physics and Deutsche Physikalische Gesellschaft

respectively (increasing unidirectionality at the price of decreasing efficiency [31]). Thus, the standard PPS-DFB Raman fiber laser performance in terms of efficiency and unidirectionality is still limited.

To improve the PPS-DFB laser performance, engineering the grating's coupling distribution function and the π-phase-shift position for a given FBG length, is necessary [7, 15, 20, 31]. The grating's ideal coupling as a function of distance results in extreme power conversion from pump to signal, i.e., efficiency as well as unidirectionality. The π-phase-shift position is also the place at which the coupling function changes sign. The longitudinal variation of the coupling coefficient can be translated into a change in refractive index and inscribed in a fiber core [20, 29]. However, it is worth noting that there are significant differences between DFB rare-earth-doped-fiber lasers and DFB Raman fiber lasers. First, the gain mechanism is different. Second, the considerable Kerr nonlinearity of the fiber changes the characteristics of such DFB Raman laser including the lasing wavelength, the intra-cavity power (and consequently the nonlinearity) as well as output power. Third, an increase in nonlinear refractive index induced by thermal gradient is present. Therefore, these different features make a Raman laser a more complex system for which the design should be accompanied by solving the generalized coupled-mode equations. For instance, to increase the small Raman laser power in a PPS-DFB written in a fixed-length fiber (e.g., in a high-loss case), step-strength grating technique [31] has already been used nevertheless, it cannot be applied to general cases and a more universal technique is required. Further, the peak power at the Stokes wavelength within the cavity is increased using the previous technique which is not desirable [30]. Surprisingly, we solve here the problems using a new coupling-engineered technique considering Raman fiber laser features to realize super-efficient PPS-DFBs which may need longer FBGs. Reproducible ultra-long fiber Bragg gratings have been recently realized which provides the possibility for engineering these long gratings [34].

In this paper, first to engineer the coupling of an FBG to increase the laser efficiency and unidirectionality, a design technique for DFB lasers is developed in the linear regime, in section 2. Based on a numerical approach, we calculate the ideal intra-cavity Raman signal powers versus different pump powers for given fiber lengths. The result is used to find the proper sum and difference between the counter-propagating wave intensities, at each small segment within the length of PPS-DFB Raman fiber lasers, to calculate the coupling functions along the fiber lengths for co- and contra-directional pumping schemes. This design is achieved without any previous assumption of the FBG's coupling for a unidirectional operation. In section 3, we include the Kerr nonlinearities to better understand the behavior of Raman DFB lasers and propose a realistic design in the nonlinear regime. The modified coupling profiles for different lengths are applied to the generalized coupled-mode equations in the steady state, considering nonlinear effects, to get a desired length and corresponding coupling profile for an increased output power decreasing an intra-cavity peak power, resulting in a *super-efficient* laser. The robustness of such a laser against second-mode generation is then described. Finally, the output power reductions of *super-efficient* and *standard* PPS-DFB Raman fiber lasers due to an increase in nonlinear refractive index induced by thermal gradient in the fiber are compared and discussed.

2. FBG design for ideal intra-cavity power in linear regime

The schematic of a DFB Raman fiber laser cavity including an FBG with the length L is shown in figure 1. Assuming slowly-varying envelopes, the standard coupled-mode equations for counter-directional coupling of the electric field amplitudes in a uniform FBG can be written as [35]

$$\frac{\mathrm{d}A^{+}(z)}{\mathrm{d}z} = \kappa(z)A^{-}(z) + g(z)A^{+}(z), \tag{1}$$

$$\frac{\mathrm{d}A^{-}(z)}{\mathrm{d}z} = \kappa(z)A^{+}(z) - g(z)A^{-}(z), \tag{2}$$

where A^{+} and A^{-} are the forward and backward propagating amplitudes at the distance z, respectively, g is the amplitude gain and κ is the coupling coefficient. Considering two new parameters, $S(z)$ and $D(z)$ as the sum and difference between the counter-propagating wave intensities, they read

$$S(z) = A^{+}(z)^2 + A^{-}(z)^2, \tag{3}$$

$$D(z) = A^{+}(z)^2 - A^{-}(z)^2. \tag{4}$$

The intensities are equal to the power divided by the effective area. Multiplying equations (1) and (2) with $A^{+}(z)$ and $A^{-}(z)$, respectively, and taking the sum and difference using equations (3) and (4) and

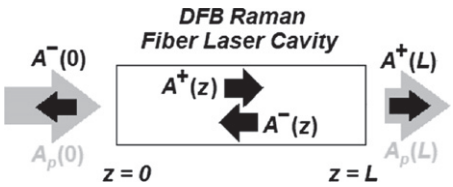

Figure 1. Schematic of a DFB Raman fiber laser cavity. The gray arrows show that the Raman pump amplitude, A_p enters from the lhs and exits from the rhs. The black arrows show the forward/backward signal amplitudes, $A^{\pm}$ within and outside of the cavity. The laser is fully unidirectional in lhs and rhs when $A^+(L) = 0$ and $A^-(0) = 0$, respectively. Please note that the boundary conditions always dictate that $A^+(0) = 0$ and $A^-(L) = 0$.

solving for $D(z)$ and $\kappa(z)$ we have

$$D(z) = D(0) + 2\int_0^z g(z')\,S(z')\,\mathrm{d}z', \tag{5}$$

$$\kappa(z) = \left[\frac{1}{2}\frac{\mathrm{d}S(z)}{\mathrm{d}z} - D(z)\,g(z)\right] / \sqrt{S(z)^2 - D(z)^2}, \tag{6}$$

where $D(0)$ is the initial value determined by boundary-conditions (see figure 1). Using equation (5), it can be shown simply that a change in $D(z)$ over an FBG (laser cavity) length, is equal to the total generated or absorbed power as $D(L) - D(0) = A^+(L)^2 + A^-(0)^2 = 2\int_0^L g(z)\,S(z)\,\mathrm{d}z$. Thus, to generate extreme output power, $S(z)$ should be increased as much as possible in different segments along the length. The boundary condition in a laser resonator at $z = 0$ dictates that $A^+(0) = 0$, thus $D(0) = -A^-(0)^2 = -S(0)$. Similarly, at $z = L$ the boundary condition requires that $A^-(L) = 0$, thus $D(L) = A^+(L)^2 = S(L)$.

For the laser to operate, the pump is situated at a wavelength, $\lambda_p = \lambda_B - \delta\lambda_s$, where λ_B is the Bragg wavelength and $\delta\lambda_s$ is the Stokes shift so that the Stokes signal wavelength is $\lambda_s = \lambda_B$. The propagation of the pump, P_p and Stokes signal power, P_S in a fiber results in pump depletion and Stokes signal amplification, described by the coupled-mode equations [36]

$$\frac{\mathrm{d}P_p(z)}{\mathrm{d}z} = -\left(g_p P_S + \alpha_p\right) P_p = D_p P_p, \tag{7}$$

$$\frac{\mathrm{d}P_S(z)}{\mathrm{d}z} = (g_s P_p - \alpha_s) P_S = G_s P_S, \tag{8}$$

where (α_p, g_p) and (α_s, g_s) are the loss and modified Raman gain coefficients for the pump and signal, respectively. Modified Raman gain coefficients for the signal and pump are given by $g_s = g_R/A_{\mathrm{eff}}$ and $g_p = g_s\lambda_s/\lambda_p$, respectively, where g_R is the Raman gain coefficient and A_{eff} is the effective mode area of the fiber. D_p and G_s are the pump depletion and signal amplification functions, respectively and the intra-cavity signal to pump change (per length) ratio is $G_s P_S / D_p P_p$ where $P_S = SA_{\mathrm{eff}}$. It is worth noting that G_s and D_p are functions of pump and signal power, respectively. Therefore, for a pump power, by sweeping the signal power, an ideal intra-cavity signal power, can be found resulting in high signal to pump change ratio, for a given length of lossy fiber. The calculations are then performed for different pump powers in order to obtain the ideal intra-cavity signal power for two different fiber lengths which have been shown in figure 2(a). The pump wavelength is chosen to be $\lambda_p = 1480$ nm resulting in a Stokes wavelength at $\lambda_s = 1576$ nm. Linear fiber loss is $\alpha_p = \alpha_s$ which is assumed to be 0.05 dB m^{-1} in the wavelength region around 1.5 μm [30]. For the fiber, the mode field diameter is $\sim$4 μm and the Raman gain coefficient is $g_R = 0.7 \times 10^{-13}$ m W^{-1} for linearly-polarized modes throughout the paper. In figure 2(a), it is seen that for a pump power of 10 W, the ideal intra-cavity signal powers are 1180 W and 527 W for the typical lengths of 42.5 cm and 97.5 cm, respectively, reaching zero for the pump power threshold of $\sim$1.9 W.

To design the DFB laser for extreme efficiency, the pump power distribution and the corresponding intra-cavity signal power, $S(z)A_{\mathrm{eff}}$ are required. We thus need these to calculate $D(z)$ and the coupling using equations (5) and (6). For a given length and an input pump power, an ideal signal power corresponding to $P_p(0)$ is found using ideal intra-cavity signal power data for different pump powers (e.g., from figure 2(a)), and considered as $P_S(0)$. Considering constant pump and signal power over a small segment of length Δz, the pump at $z = \Delta z$ is $P_p(\Delta z) = P_p(0) + \Delta P_p(0)\,\Delta z$ where $\Delta P_p(0) = -gP_S(0)\,P_p(0) - \alpha_p P_p(0)$. For this new pump value, we again find the corresponding signal power at Δz using ideal intra-cavity signal power data for various pump powers (e.g., from figure 2(a)) and calculate similarly the new pump and signal power at $z = 2\Delta z$. We continue the calculation till the end at $z = L$ to achieve the signal and pump power distribution over the whole length. The inset in figure 2(a) depicts pump power distribution versus length for a pump power of 10 W. The residual pump power at the rhs is almost 1.9 W for a loss of 0.05 dB m^{-1}.

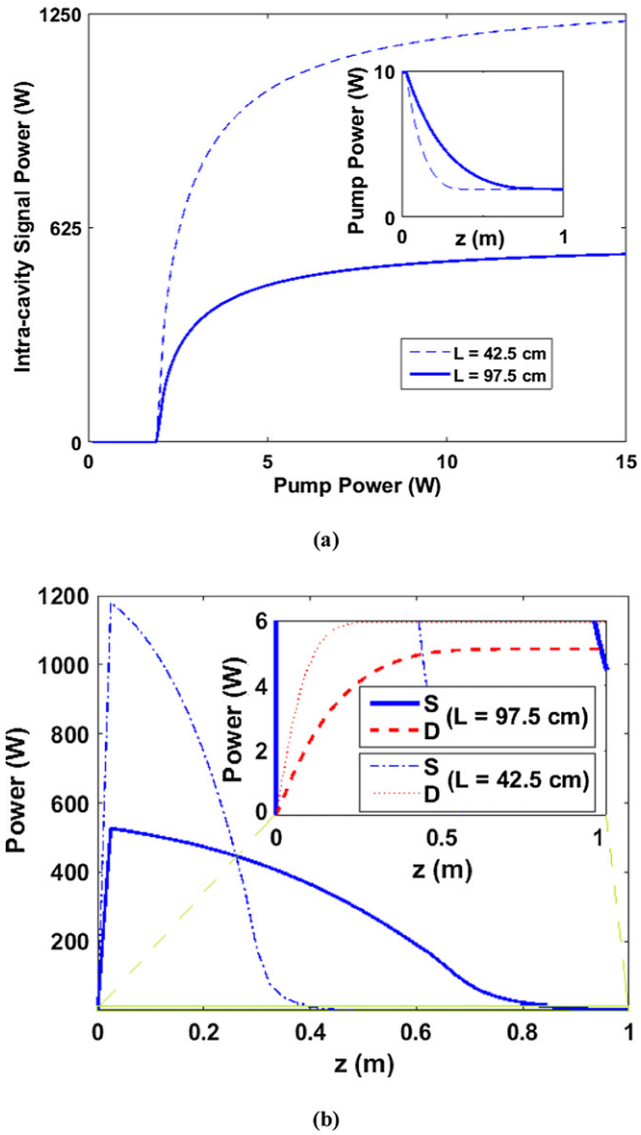

Figure 2. (a) Ideal intra-cavity signal power versus pump power for two different fiber cavity lengths. Inset: pump power distribution versus distance, $P_p(z)$ for two various lengths of DFB fiber lasers. (b) The intra-cavity signal power, $S(z)A_{\text{eff}}$ versus length for two engineered DFB fiber lasers with different lengths. The inset is the green zoomed-in part showing the intersections of power curves namely, $S(z)A_{\text{eff}}$ and $D(z)A_{\text{eff}}$ at 42.5 cm and 97.5 cm for two different fiber lengths.

To calculate $D(z)$ using equation (5), we have to define the initial value $D(0)$ according to the boundary condition at $z = 0$ (see figure 1). Here, for a fully unidirectional laser in the rhs (co-directional pumping), we have $D(0) = 0$ as no power exits the cavity from the lhs. The second boundary condition on the rhs, expressed as $S(L) = D(L)$, should then be satisfied. Alternatively, for a fully unidirectional laser in the lhs (contra-directional pumping), $S(0) = -D(0)$ so that $S(L) = D(L) = 0$ is satisfied.

Figure 2(b) shows the ideal power, $S(z)A_{\text{eff}}$ versus length for the pump power of 10 W and two different lengths of 42.5 cm and 97.5 cm for which the intra-cavity power reaches 1180 W and 527 W, respectively. Thus, a shorter length leads to a higher efficiency at the price of larger intra-cavity peak power. The inset in figure 2(b) demonstrates that the $S(z)A_{\text{eff}}$ and $D(z)A_{\text{eff}}$ power curves intersect at 42.5 cm and 97.5 cm dictated by the boundary conditions for a fully unidirectional laser in the rhs. For the lengths of 42.5 cm and 97.5 cm, the rhs signal powers are 5.87 W and 5.12 W, respectively.

The engineered PPS-DFB Raman fiber laser consists of a fiber Bragg grating with a length of L and coupling of $\kappa(z)$. By inserting $S(z)$ and $D(z)$ in equation (6), the proper coupling function, $\kappa(z)$ between 0 and $L = 97.5$ cm is calculated. The coupling defines the periodic perturbation and for a sinusoidally varying refractive-index modulation is equal to $\kappa(z) = \pi\Delta n(z)/\lambda_B$ where $\Delta n(z)$ is the amplitude of the refractive index modulation in the grating [2]. The grating is designed with the period of $\Lambda = \lambda_B/2n_{\text{eff}}$ where n_{eff} is the effective refractive index of the propagating mode. It is worth noting as the coupling and consequently average refractive index of the mode changes, the Bragg wavelength is detuned which is considered later in section 3 via the detuning [1].

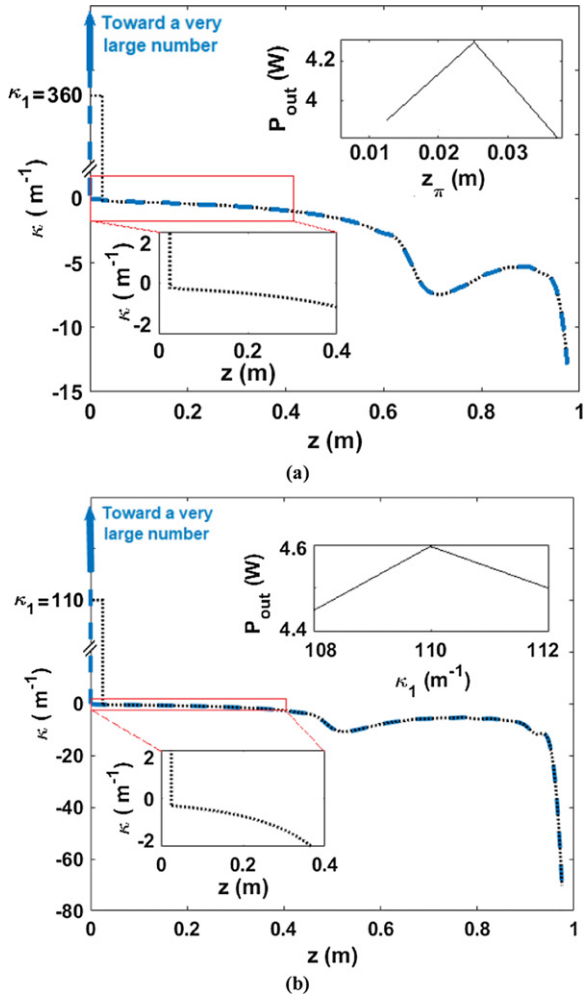

Figure 3. Coupling versus length for (a) co-pumping and (b) contra-pumping configurations. Dashed line shows the ideal coupling function for full unidirectionality in the linear regime using the numerical calculation on equations (1) and (2) in section 2. The dotted line shows a typical modified coupling function for the *best* unidirectionality in the nonlinear regime used in the simulation of equations (9) and (11) in section 3, to reach maximum (a) rhs and (b) lhs output power, using the *best* coupling coefficient, κ_1 between 0 and $z_\pi = 2.5$ cm. The lower insets show the red zoom-in parts from $z = 0$ to $z = 40$ cm. The upper inset in (a) shows the simulated rhs output power versus phase-shift positions where for the numerical parameter $\kappa_1 = 360$ m^{-1} the output power is maximized (within the used resolution) for a value of z_π between 1.25 cm and 3.75 cm at 2.5 cm. Due to computation time limitation, the z resolution is limited to 1.25 cm. The upper inset in (b) shows the simulated lhs output power versus coupling for $z_\pi = 2.5$ cm with the *best* output power for $\kappa_1 = 110$ m^{-1} for the κ_1 resolution of 2 m^{-1}.

Figures 3(a) and (b) (*blue dashed curves*) illustrate the ideal coupling versus length for co- and contra-pumping configurations, respectively, for a pump power of 10 W and loss of 0.05 dB m^{-1}. A very large coupling is necessary at $z = 0$ due to the lhs boundary condition required for fully unidirectional operation. The sign change in the coupling can then be obtained by introducing a π-shift in the grating in the phase of the refractive index modulation along the FBG length at $z = z_\pi$. The initial part of the grating between $z = z_\pi$ and the minimum point on the saddle-like part of the curve at $z = (71\text{ cm} \,\&\, 52\text{ cm})$ represent increasing $|\kappa|$ from 0 to $\left(7\text{ m}^{-1}\ \&\ 10.7\text{ m}^{-1}\right)$, in figures 3(a) and (b) required for the signal power reduction over the central region. The final part of the grating between the minimum point on the saddle-like part of the curve and the fiber end initially signifies a decreasing $|\kappa|$ from $\left(7\text{ m}^{-1}\ \&\ 10.7\text{ m}^{-1}\right)$ to $\left(5\text{ m}^{-1}\ \&\ 5.2\text{ m}^{-1}\right)$ and then increasing $|\kappa|$ exponentially from $\sim$0.05 m to $\left(12\text{ m}^{-1}\ \&\ 70\text{ m}^{-1}\right)$ keeps the signal distribution at the perfect value till the rhs boundary conditions are met at the fiber end.

Our coupling distribution for extreme efficiency also shows an analogy to rapid adiabatic passage [37]. It is a technique already used in the domain of frequency conversion to solve the need of high efficiency [37] and is being used in other fields of optics [38–41]. Under this technique, adiabatic variation of the coupling coefficient along the propagation length of (lossless/lossy) fiber allows (full/extreme) transfer of energy from a pump to a Stokes signal. With uniform FBGs, this can be done by changing the index of the modulation pattern, which has a direct influence on the coupling.

3. FBG design using best realistic couplings considering nonlinearities and thermal gradient

In practice, nonlinearities have an important effect in decreasing the intra-cavity and output power of DFB Raman fiber lasers [29–31]. Therefore, to evaluate the laser with realistic parameters, the generalized coupled mode equations in the steady state for the slowly varying amplitudes of the pump wave (A_p) and the forward Stokes($A_s{}^+$), and backward Stokes ($A_s{}^-$) waves, in the presence of the Kerr nonlinearity, should be taken into account which can be written as [2]

$$\frac{\partial A_p}{\partial z} = \left\{\left[-\frac{g_p}{2}\left(|A_s{}^+|^2 + |A_s{}^-|^2\right) - \frac{\alpha_p}{2}\right] + i\gamma_p\left[|A_p|^2 + 2|A_s{}^+|^2 + 2|A_s{}^-|^2\right]\right\}A_p, \tag{9}$$

$$\frac{\partial A_s{}^+}{\partial z} = \left\{\left[\frac{g_s}{2}|A_p|^2 - \frac{\alpha_s}{2}\right] - i\left[-\gamma_s\left(2|A_p|^2 + |A_s{}^+|^2 + 2|A_s{}^-|^2\right) - \delta\right]\right\}A_s{}^+ + i\kappa A_s{}^-, \tag{10}$$

$$-\frac{\partial A_s{}^-}{\partial z} = \left\{\left[\frac{g_s}{2}|A_p|^2 - \frac{\alpha_s}{2}\right] - i\left[-\gamma_s\left(2|A_p|^2 + 2|A_s{}^+|^2 + |A_s{}^-|^2\right) - \delta\right]\right\}A_s{}^- + i\kappa A_s{}^+. \tag{11}$$

It should be noted that equations (10) and (11) are not simple extended forms of equations (1) and (2). The squares of the absolute values of the slowly varying amplitudes are equal to the powers of the corresponding waves, i.e., $|A_p|^2 = P_p$ and $|A_s{}^\pm|^2 = P_s{}^\pm$. The nonlinear coefficients are defined by $\gamma_s = 2\pi n_2/\lambda_s A_{eff}$ and $\gamma_p = \gamma_s\lambda_s/\lambda_p$ where $n_2 = 3.2 \times 10^{-20}$ m^2 W^{-1} is the nonlinear refractive index. The detuning of the signal from the Bragg frequency ω_B is $\delta = n(\omega - \omega_B)/c$, where ω is the carrier frequency of the slowly varying amplitudes $A_s{}^\pm$, n is the refractive index of the fiber core and c is the speed of light in vacuum. Here, we consider a continuous-wave linearly-polarized pump of power $P_p(0)$ is launched into the fiber at $z = 0$ and the polarization state of the pump wave is maintained all the way to $z = L$. As the pump is far from the Bragg resonance and does not interact with the grating, only the Stokes waves are coupled by the grating. Later for the simulation and design, we solve the coupled-mode equations (9) and (11) using the Runge–Kutta method [31, 42] considering the other fiber parameters already utilized in section 2. Also, it should be noted that $2|A_p|^2$ is dominant for the regions where the approximation $|A_s{}^+|^2 \approx |A_s{}^-|^2$ does not hold.

To realize an engineered PPS-DFB Raman fiber laser, a very large coupling at $z = 0$ is impractical. A solution to the problem in (co- & contra-) pumping configuration is to decrease the unidirectionality by permitting a very small output power in the (lhs & rhs), defined by an increase in the signal power over a short length which is the distance between $z = 0$ and $z = z_\pi$. It should be noted that we can select a *best* coupling for a given short length, z_π resulting in maximizing output power (within the used resolution) to prove the efficiency supremacy of engineered PPS-DFB over a *standard* one with the same strength [31]. Therefore, the ideal coupling profiles for a given length (see figure 3, blue dashed curves), obtained using the aforesaid technique (section 2) and modified by feasible *best* coupling, κ_1 between $z = 0$ and $z = z_\pi$ are then applied to equations (9) and (11) to get the largest output power. The *best* modified coupling profiles for co- and contra-pumping 97.5 cm-long *super-efficient* PPS-DFB lasers are depicted using *black dotted curves* in figures 3(a) and (b), respectively. The simulation results have also been reflected in the upper insets in figure 3 showing output power versus z_π and κ_1. At the cost of a small increase in the contra-directional signal powers, the *best* realistic coupling for the PPS location at 2.5 cm are calculated to be 360 m^{-1} and 110 m^{-1} for the largest output power (within the used resolution), in co- & contra-pumping configuration, respectively. Those flat- κ parts are the grating section necessary for the increase in the signal power toward the peak which can be readily obtained with the fiber properties and grating writing technology. Moreover, the zoomed-in parts as the lower insets in figure 3 show the jump of coupling from a large positive to a small negative value at $z_\pi = 2.5$ cm. Our simulations demonstrate that although the output power is increased from 4.32 W for the co-directional pumping to 4.6 W for the contra-directional pumping, it results in increasing the peak intra-cavity power from 345 W to 542 W. From this point forward, we focus on co-directional pumping generating less intra-cavity power for almost the same output power.

Figure 4(a) shows the rhs output power and intra-fiber peak power versus fiber length for 10 W-pumped engineered PPS-DFBs with and without nonlinearities, considering the *best* coupling for each length. It is seen in figure 4(a) that nonlinearities in general result in decreasing the output power and intra-fiber peak power, however, increasing the fiber length initially leads to less intra-fiber peak power and consequently less nonlinearity which enhances the output power. By reaching the *best* length, the *best* output power is attained and for longer lengths the nonlinearity is strong enough to again decrease the output power. For a 97.5 cm-long *super-efficient* PPS-DFB with $\int_0^L |\kappa|\,dz \sim 12$, the *best* output power of 4.32 W (with 56.5 dB unidirectionality), intra-cavity peak power of 340 W and output unused-pump power of 3.56 W are achieved. The results can be compared with those obtained for a 10 W-pumped *standard* PPS-DFB [31]

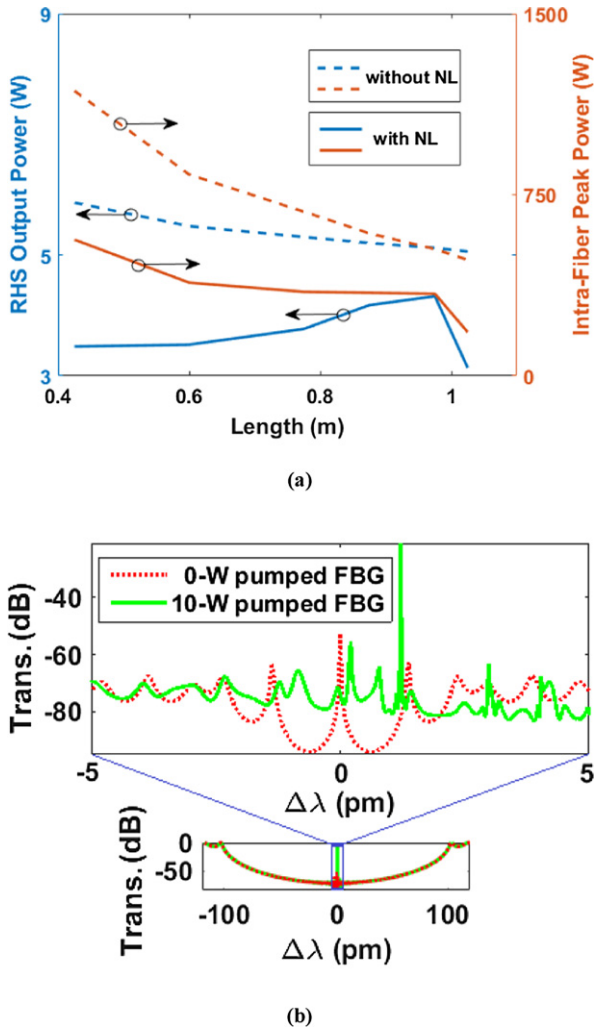

Figure 4. (a) rhs Output power and intra-fiber peak power versus fiber length for a 10 W pump power, without and with nonlinearities. (b) The transmission (including a zoomed-in section) for a 97.5 cm-long FBG without and with pumping, demonstrating single-mode operation.

with the strength, $\kappa L = 12$ where the *best* output power of 2.88 W (with 12.1 dB unidirectionality), minimum intra-cavity peak power of 5540 W and output unused-pump power of 5.73 W are obtained. Therefore, a 50% increase in the laser efficiency (the power ratio of the output signal to input pump), 44 dB reduction in contra-directional lasing power, 15.3 times drop in intra-cavity signal power and 37.9% decrease in unused pump power are found. Furthermore, figure 4(b) shows the transmission for a 97.5 cm-long *super-efficient* PPS-DFB without and with a 10 W pumping, where the detuning and distortion in the latter are due to the Kerr nonlinearities. The laser provides single-mode operation with a ∼1.2 pm (∼146 MHz) detuning, when pumped which is 10 times less than that of the *standard* PPS-DFB (∼1.44 GHz) [31]. The linewidths are calculated as 807 KHz and 976 KHz for the *super-efficient* and *standard* PPS-DFB [31], respectively. It is worth noting that keeping the fiber length <1 m ensures that the grating's uniformity is maintained along the length and the coupling of the flat-κ part (e.g., ∼360 m^{-1}) can be fabricated in practice.

For both above-mentioned PPS-DFBs, the laser has only one longitudinal mode at 10 W, however, using higher input pump power, i.e., 15 W, results in the generation of the second longitudinal mode. For a 15 W pump power, the fundamental and second-order longitudinal modes in the *super-efficient* PPS-DFB are shown in figure 5(a), where the modes are distributed more widely within the cavity. For comparison, the fundamental and second-order longitudinal modes in the *standard* PPS-DFB are shown in figure 5(b), where the modes are distributed narrowly within the cavity with less overlapping. The larger overlap in the engineered design results in gain saturation by the fundamental mode, thus, the higher order mode start lasing but with much less power due to the lack of enough gain. For a 15 W pump power, the laser side-mode suppression ratio [8] and mode frequency-distance (see the insets in figures 5) [31] for the *super-efficient* and *standard* PPS-DFB are 10.7 dB/83 MHz and 2.6 dB/659 MHz, respectively.

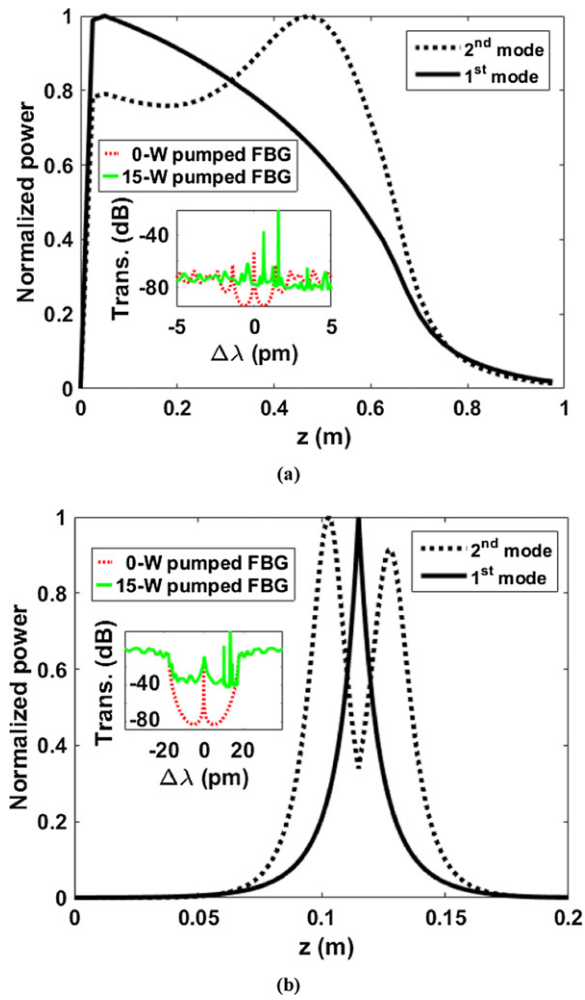

Figure 5. Normalized fundamental and second-order longitudinal modes for (a) a 97.5 cm-long *super-efficient* PPS-DFB and (b) 20 cm-long *standard* PPS-DFB, pumped by 15 W. The insets show the transmission without and with pumping, demonstrating double-mode operation.

Finally, we have already demonstrated that there is a degradation in the output power of PPS-DFB Raman fiber laser due to an increase in nonlinear refractive index [43] induced by thermal gradient along the FBG [30]. The thermal gradient is modeled considering that a temperature variation will lead to an increase in the refractive index of the fiber and thus an increase in phase. By approximating heating as being linear with local intensity we increased the nonlinear refractive index by an amount of $n_2^{\mathrm{th}} = \frac{\mathrm{d}n}{\mathrm{d}T}\frac{\mathrm{d}T}{\mathrm{d}I}$ to represent its contribution to the effective nonlinear refractive index as $n_2^{\mathrm{eff}} = n_2 + n_2^{\mathrm{th}}$ where T is the temperature, and I is the optical intensity of the lasing mode [30]. The effect of an increased nonlinear refractive index on output power for the 10 W-pumped *super-efficient* and *standard* PPS-DFB lasers (used in figures 5) is simulated and shown in figure 6. As can be seen, an increase of up to $\sim$ 18 times in effective nonlinearity ratio, n_2^{eff}/n_2 can decrease the output power by nearly an order of magnitude, however, the output power for the former is still more than 50% of the latter, over all nonlinearity ratios. The inset in figure 6 also shows that the intra-cavity peak power decreases with the enhancement of nonlinearity and for the *super-efficient* PPS-DFB is an order of magnitude smaller than the *standard* PPS-DFB over the range. There is a good way to estimate the magnitude of thermal nonlinear refractive index and consequently the effective nonlinearity ratio to find the peak and output power in figure 6. By solving the heat-transport equation under steady-state conditions, it can be shown [44] that for a continuous-wave laser beam in a core of radius a, the largest thermal-induced nonlinear refractive index can be approximated as $n_2^{\mathrm{th}} = \left(\frac{\mathrm{d}n}{\mathrm{d}T}\right)\alpha a^2/k$ where α is the absorption coefficient and k is the thermal conductivity. Assuming $\alpha \sim 0.01\ \mathrm{m}^{-1}$, $k \sim 1.38\ \mathrm{W\ m^{-1}\ K^{-1}}$ and $\frac{\mathrm{d}n}{\mathrm{d}T} \sim 10^{-5}\ \mathrm{K}^{-1}$, the thermally-induced nonlinear refractive index is $n_2^{\mathrm{th}} = 2.9 \times 10^{-19}$ and effective nonlinearity ratio is $n_2^{\mathrm{eff}}/n_2 \sim 10$. The intra-cavity peak and output powers for *super-efficient* PPS-DFB lasers are then 44 W and 0.97 W, respectively.

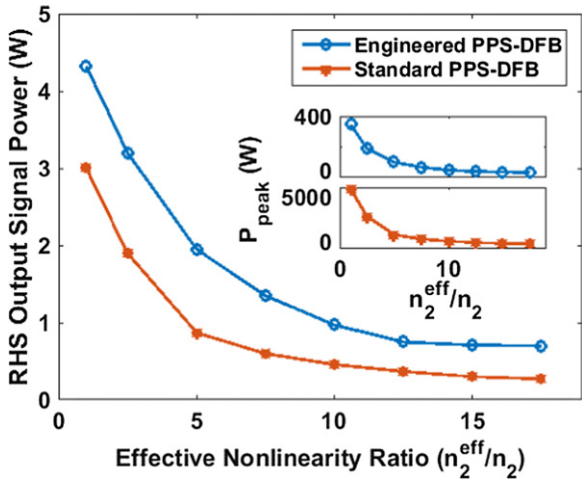

Figure 6. rhs Output power versus effective nonlinearity ratio for engineered *super-efficient* and *standard* PPS-DFB. The inset shows the intra-cavity peak power versus effective nonlinearity ratio.

4. Conclusion

A new technique was presented to design highly-efficient and -unidirectional DFB Raman fiber lasers based on a π-phase-shifted coupling-engineered fiber Bragg grating. For a given length and pump power in co- and contra-directional-pumping, the sum and difference distributions were calculated resulting in finding the grating's ideal coupling function. The steady-state behavior of the laser was simulated for a realistic modified coupling function to evaluate its real output power and intra-fiber peak power considering nonlinearities. For $\sim$1 m-long co-directional-pumped, *super-efficient* PPS-DFB, a considerable increase in the laser efficiency, and significant reduction in contra-directional lasing power, peak power of intra-cavity signal and output unused-pump power are found compared to those in a *standard* PPS-DFB with the same strength. Moreover, an increased overlap between two modes in the *super-efficient* design promotes robustness against second mode generation and guarantees the stability of the single-mode for pump powers up to $\sim$15 W. Although an increased nonlinear refractive index due to thermal gradient decreases the output power of PPS-DFB lasers, the *super-efficient* laser shows a better performance than the *standard* one.

We have already overcome several issues related to implementing such varying coupling-coefficient profiles discussed in this article, including a pi-phase shift (i.e., apodized PPS-DFB) for short fibers [28, 29] and we hope to implement the current designs in long FBGs using our novel fabrication technique to realize meter long devices [34]. The sensitivity of the laser's performance to parameter deviations is also something under further examination for a future publication.

Acknowledgments

This work has been supported by the Natural Sciences and Engineering Research Council of Canada (NSERC) program.

References

[1] Kashyap R 2010 *Fiber Bragg Gratings* 2nd edn (New York: Academic)
[2] Perlin V E and Winful H G 2001 Distributed feedback fiber Raman laser *IEEE J. Quantum Electron.* **37** 38–47
[3] Blanchard R *et al* 2011 Gratings with an aperiodic basis: single-mode emission in multi-wavelength lasers *New J. Phys.* **13** 113023
[4] Utaka K, Akiba S, Sakai K and Matsushima Y 1984 λ/4-shifted InGaAsP/InP DFB lasers by simultaneous holographic exposure of positive and negative photoresists *Electron. Lett.* **20** 1008–10
[5] McCall S and Platzman P 1985 An optimized π/2 distributed feedback laser *IEEE J. Quantum Electron.* **21** 1899–904
[6] Usami M, Akiba S and Utaka K 1987 Asymmetric λ/4-shifted InGaAsP/InP DFB lasers *IEEE J. Quantum Electron.* **23** 815–21
[7] Li S, Guo R, Li L, Shi Y, Lu J, Lu L, Zheng J and Chen X 2014 Experimental demonstration of DFB semiconductor lasers with varying longitudinal parameters *Opt. Express* **22** 4059–64
[8] Carroll J, Whiteaway J and Plumb D 1998 *Distributed Feedback Semiconductor Lasers* (Piscataway: The Institution of Electrical Engineers)
[9] Kringlebotn J T, Archambault J-L, Reekie L and Payne D N 1994 Er^{3+}:Yb^{3+}-codoped fiber distributed-feedback laser *Opt. Lett.* **19** 2101–3

[10] Canning J and Sceats M G 1994 π-phase shifted periodic distributed structures in optical fibers by UV post-processing *Electron. Lett.* **30** 1244–5
[11] Loh W H and Laming R I 1995 1.55 μm phase-shifted distributed feedback fibre laser *Electron. Lett.* **31** 1440–2
[12] Asseh A, Margulis W, Sandgren S, Kringlebotn J T, Edwall G, Sahlgren B, Storoy H and Stubbe R 1995 10 cm Yb_3 + DFB fibre laser with permanent phase shifted grating *Electron. Lett.* **31** 969–70
[13] Sejka M, Hübner J, Varming P and Kristensen M 1995 Distributed feedback $Er_3{}^+$-doped fibre laser *Electron. Lett.* **31** 1445–6
[14] Lauridsen V C, Povlsen J H and Varming P 1998 Design of DFB fibre lasers *Electron. Lett.* **34** 2028–30
[15] Yelen K, Zervas M N and Hickey L M B 2005 Fiber DFB lasers with ultimate efficiency *IEEE J. Lightwave Technol.* **23** 32–43
[16] Babin S A, Churkin D V, Ismagulov A E, Kablukov S I and Nikulin M A 2007 Single frequency single polarization DFB fiber laser *Laser Phys. Lett.* **4** 428–32
[17] Skvortsov M I, Wolf A A, Dostovalov A V, Vlasov A A, Akulov V A and Babin S A 2018 Distributed feedback fiber laser based on a fiber Bragg grating inscribed using the femtosecond point-by-point technique *Laser Phys. Lett.* **15** 035103
[18] Behzadi B, Aliannezhadi M, Hossein-Zadeh M and Jain R K 2017 Design of a new family of narrow-linewidth mid-infrared lasers *J. Opt. Soc. Am.* B **34** 2501–13
[19] Jiang M, Zhou P and Gu X 2018 Ultralong π-phase shift fiber Bragg grating empowered single-longitudinal mode DFB phosphate fiber laser with low-threshold and high-efficiency *Sci. Rep.* **8** 13131
[20] Guo K, He J, Yang K, Zhang Z, Xu X, Du B, Xu G and Wang Y 2019 Symmetric step-apodized distributed feedback fiber laser with improved efficiency *IEEE Photon. J.* **11** 1–11
[21] Abedin K S, Westbrook P S, Nicholson J W, Porque J, Kremp T and Liu X 2012 Single-frequency Brillouin distributed feedback fiber laser *Opt. Lett.* **37** 605–7
[22] Winful H G, Kabakova I V and Eggleton B J 2013 Model for distributed feedback Brillouin lasers *Opt. Express* **21** 16191–9
[23] Hu Y and Broderick N G R 2009 Improved design of a DFB Raman fibre laser *Opt. Commun.* **282** 3356–9
[24] Westbrook P S, Abedin K S, Nicholson J W, Kremp T and Porque J 2011 Raman fiber distributed feedback lasers *Opt. Lett.* **36** 2895–7
[25] Shi J, Alam S-u. and Ibsen M 2012 Highly efficient Raman distributed feedback fibre lasers *Opt. Express* **20** 5082–91
[26] Shi J, Alam S-u. and Ibsen M 2012 Sub-watt threshold, kilohertz-linewidth Raman distributed-feedback fiber laser *Opt. Lett.* **37** 1544–6
[27] Shi J, Alam S-u. and Ibsen M 2013 Ultrawide-range four-wave mixing in Raman distributed-feedback fiber lasers *Opt. Lett.* **38** 944–6
[28] Loranger S, Karpov V, Schinn G W and Kashyap R 2017 Single-frequency low-threshold linearly polarized DFB Raman fiber lasers *Opt. Lett.* **42** 3864–7
[29] Loranger S and Kashyap R 2018 Efficiency increase of distributed feedback Raman fiber lasers by dynamic control of the phase shift *Opt. Lett.* **43** 5705–8
[30] Loranger S, Tehranchi A, Winful H and Kashyap R 2018 Realization and optimization of phase-shifted distributed feedback fiber Bragg grating Raman lasers *Optica* **5** 295–302
[31] Tehranchi A, Loranger S and Kashyap R 2018 Engineered π-phase-shifted fiber Bragg gratings for efficient distributed feedback Raman fiber lasers *IEEE J. Quantum Electron.* **54** 1600307
[32] Shi J, Horak P, Alam S-u and Ibsen M 2014 Detailed study of four-wave mixing in Raman DFB fiber lasers *Opt. Express* **22** 22917–24
[33] Headley C and Agrawal G P 2005 *Raman Amplification in Fiber Optical Communication Systems* (Amsterdam: Elsevier)
[34] Loranger S, Lambin-Iezzi V and Kashyap R 2017 Reproducible ultra-long FBGs in phase corrected non-uniform fibers *Optica* **4** 1143–6
[35] Ghatak A and Thyagarajan K 1998 *An Introduction to Fiber Optics* (Cambridge: Cambridge University Press)
[36] Agrawal G P 2013 *Nonlinear Fiber Optics* 5th edn (New York: Academic)
[37] Suchowski H, Prabhudesai V, Oron D, Arie A and Silberberg Y 2009 Robust adiabatic sum frequency conversion *Opt. Express* **17** 12731–40
[38] Aashna P and Thyagarajan K 2016 Highly efficient broadband waveguide adiabatic polarization converter with apodization *IEEE Photon. Technol. Lett.* **28** 2609–12
[39] Pascual-Winter M F, Tongning R-C, Chanelière T and Le Gouët J-L 2013 Securing coherence rephasing with a pair of adiabatic rapid passages *New J. Phys.* **15** 055024
[40] Miao Q and Zheng Y 2016 Single-photon emission of two-level system via rapid adiabatic passage *Sci. Rep.* **6** 32827
[41] Kaldewey T, Kuhlmann A V, Valentin S R, Ludwig A, Wieck A D and Warburton R J 2018 Far-field nanoscopy on a semiconductor quantum dot via a rapid-adiabatic-passage-based switch *Nat. Photon.* **12** 68–72
[42] Iezzi V L, Büttner T F S, Tehranchi A, Loranger S, Kabakova I V, Eggleton B J and Kashyap R 2016 Temporal characterization of a multi-wavelength Brillouin-erbium fiber laser *New J. Phys.* **18** 055003
[43] Dohnalová K *et al* 2008 Closely packed luminescent silicon nanocrystals in a distributed-feedback laser cavity *New J. Phys.* **10** 063014
[44] Boyd R W 2008 *Nonlinear Optics* 3rd edn (New York: Academic)